CHAPTER 3: Dielectric Relaxations in $Ho_2Ti_2O_7$ and $Dy_2Ti_2O_7$

3.1 Introduction

As discussed in the chapter 1, in spite of cetrosymmetric $Fd\bar{3}m$ space group, $Ho_2Ti_2O_7$ and $Dy_2Ti_2O_7$ shows multiple ferroelectric transitions at different temperatures [87]–[90]. Dong et al. performed pyroelectric studies on polycrystalline HTO compound, which shows two ferroelectric transitions at ~60 K and ~23 K [87]. Whereas, in the single crystal of HTO only one transition at ~28K has been observed [89]. On the other hand in polycrystalline DTO, two ferroelectric transitions at ~25K and ~13K have been observed by Lin et al. [88]. In these studies, it have been concluded that ferroelectric transitions observed at ~60 K (in polycrystalline) & ~28 K (in single crystal) of HTO and ~25 K in polycrystalline DTO has structural origin [87]–[89]. Whereas, low-temperature ferroelectric transition ~23 K (for HTO) and ~13 K (for DTO) has been dedicated to originating from the magnetism of these systems [87], [88]. The presence of ferroelectricity necessarily implies symmetry lowering from cubic $Fd\bar{3}m$ down to a non-centrosymmetric space group (tetragonal, trigonal or lower). The symmetry analysis of $Fd\bar{3}m$ space group suggests that in these compounds gyrotropic order, which belongs to the A_{1u} irreducible representation of the O_h point group, is incompatible with structural order parameters [97]. Due to this incompatibility, having a structural origin of ferroelectricity is quite unusual, however magnetism induced ferroelectricity may be possible in these compounds. In this chapter, a detailed investigation on the nature and origin of ferroelectric transitions observed in HTO and DTO above the spin ice regime has been presented.

3.2 Results and Discussion

3.2.1 Structural analysis

The HRXRD pattern of HTO, DTO, HTFO, and HFTO samples as shown in figure 2.2 and 2.3 has been analyzed using Rietveld analysis. The Rietveld fitting in the standard setting is shown in figure 3.1. For pyrochlore structure having space group $Fd\bar{3}m$, other than the usual profile parameters, variable structural parameters are- lattice constant a, x coordinate of the 48f-site and isotropic thermal parameters. The obtained structural parameters and fitting parameters are listed in table 3.1. The obtained fit is remarkably good indicating that the samples are defect free and having stoichiometry as intended. However, for Fe-substituted compositions (especially for B-site substituted), charge compensating oxygen deficiency may be generated but its effect is negligible on the crystal structure due to larger structural stability of these compound. The so obtained structural data has been used for the calculation of bond angle and bond lengths of HTO, DTO, HTFO and HFTO.

Table 3.1: Details of structural refinement as obtained from high-resolution x-ray diffraction. Compound, lattice constant, variable coordinate x in the 48f-site, R-factors (R_p, R_{wp} and R_e) and goodness of fit χ^2.

Compound	a (Å)	x (48f)	R_p	R_{wp}	R_e	χ^2
HTO	10.1006(1)	0.324(2)	14.8	14.6	6.86	4.55
DTO	10.1270(1)	0.320(2)	21.9	15.4	9.82	2.47
HTFO	10.1013(4)	0.325(1)	14.4	13.5	7.24	3.47
HFTO	10.0804(1)	0.327(1)	21.4	18.1	9.03	4.00

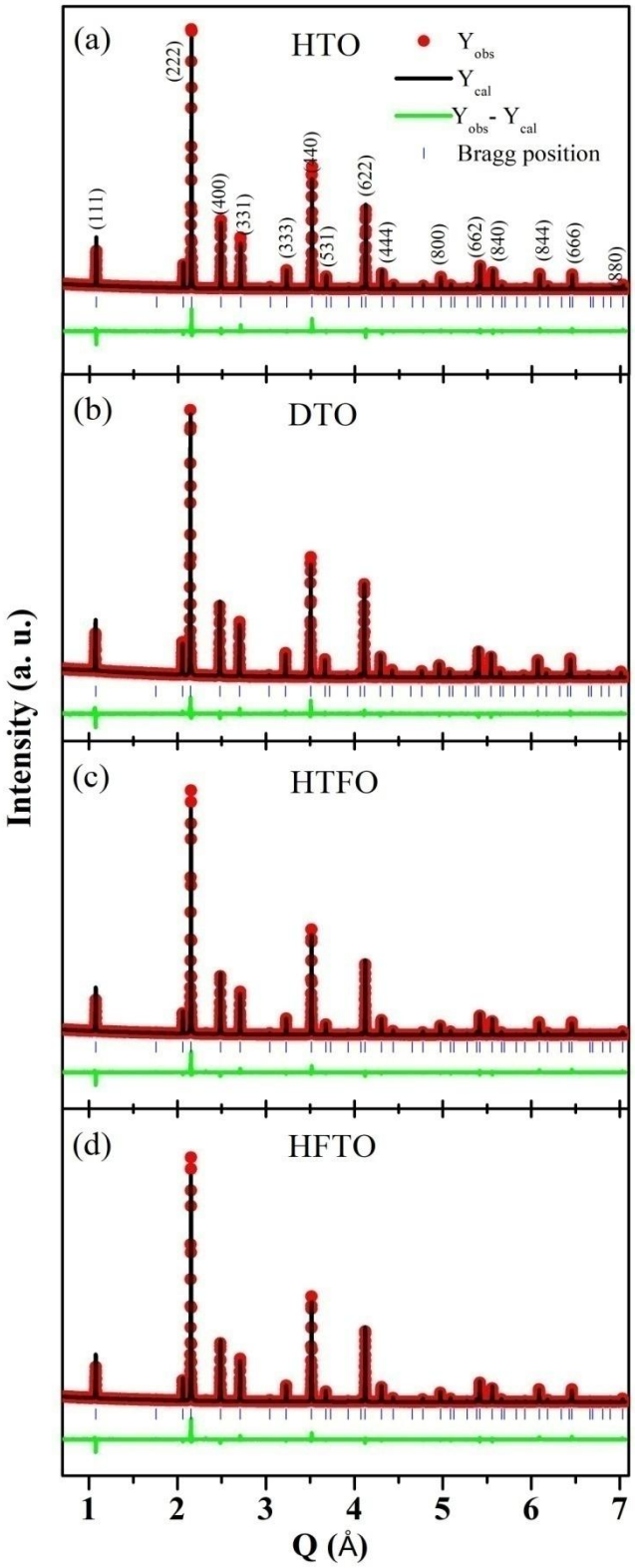

Figure 3.1: Rietveld fit of the room temperature high resolution x-ray diffraction pattern of polycrystalline (a) $Ho_2Ti_2O_7$; (b) $Dy_2Ti_2O_7$; (c) $Ho_2Ti_{1.85}Fe_{0.15}O_7$ and (d) $Ho_{1.8}Fe_{0.2}Ti_2O_7$.

3.2.2 Dielectric analysis

Temperature-dependent dielectric measurements have been performed in a frequency range of 0.5 to 400 kHz for both HTO and DTO as explained in section 2. 2.2. Figure 3.2 shows the plot of real (ε') and imaginary (ε") part of relative dielectric permittivity vs temperature at different frequencies. It has been found that both HTO and DTO show two successive dielectric relaxations in the temperature range 87-127 K and 34-49 K respectively. A broad peak develops below ~30 K up to lowest measured temperature. At 1 kHz, relaxations are observed at 90 K and 36 K in case of HTO, while in case of DTO these dielectric relaxations are observed at 92.5 K and 37 K. The ε" has a tendency to shift with increasing frequency. In this case also ε" show an offset with varying frequency. For HTO; the shift is from 0.025 to 2 as one increase the frequency from 10 kHz and 400 kHz. Similarly, for DTO the offset values change from 0.05 to 2.5 with increasing frequency from 10 kHz and 400 kHz. For 10 kHz frequency, the y-scale value for ε" lies between 0.025-0.8 and 0.05-0.5 for HTO and DTO, respectively. It has been found that dielectric relaxation (~90 K and ~36 K) in HTO and DTO shows large frequency dispersion. The peak temperature $T_{m'}$ for ε' and $T_{m''}$ for ε" shift towards higher temperature side with increasing frequency. This represents a typical feature of diffuse/relaxor nature of the dielectric relaxation. The conclusive way to determine the diffuseness of a dielectric relaxation of the compound, through the obtained value of γ in equation 3.1 [111]

$$\frac{1}{\varepsilon'} - \frac{1}{\varepsilon'_m} = \frac{(T - T_{m'})^{\gamma}}{C'} \tag{3.1}$$

Where, γ and C' are constants. For normal phase transitions (obeying Curie-Weiss law) one gets γ= 1; for relaxor phase transitions one gets γ= 2; while 1<γ<2 corresponds to the diffuse

phase transitions. In equation (3.1) values of ε'_m and $T_{m'}$ are the maxima of the ε' and its corresponding temperature, respectively.

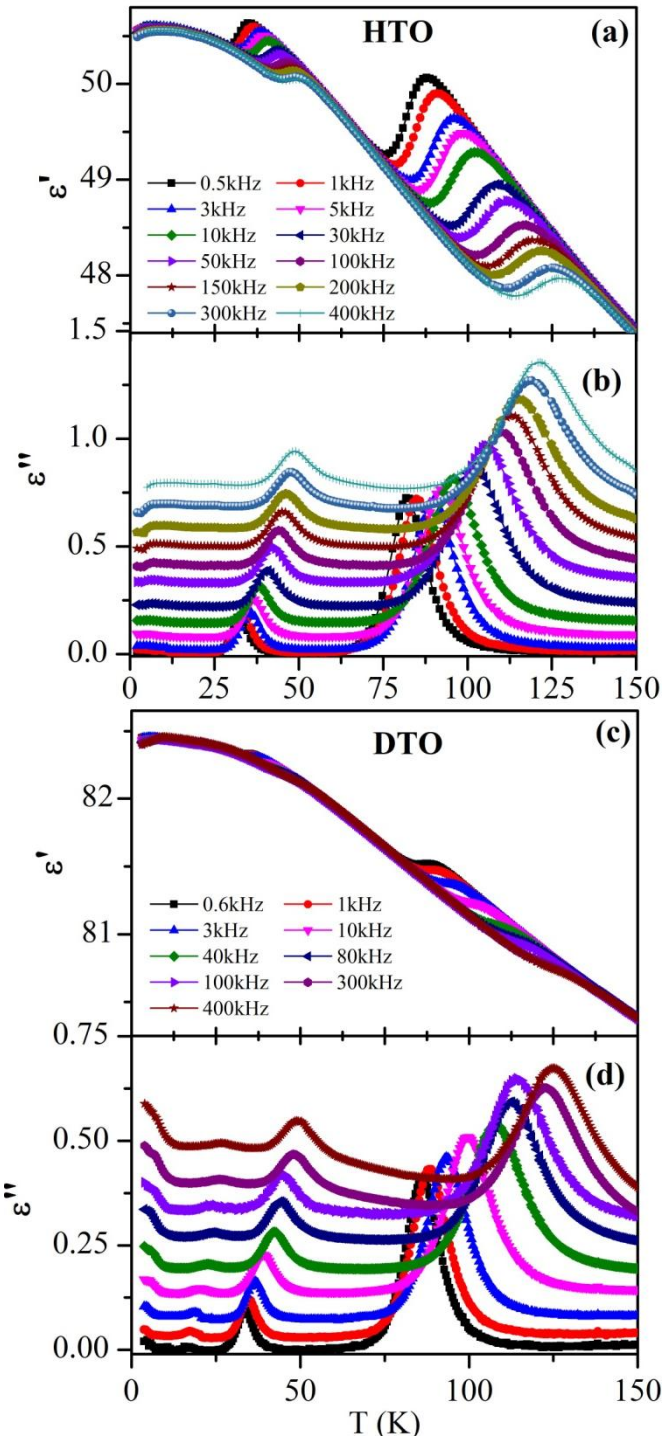

Figure 3.2: Temperature dependence of the real (ε') and imaginary (ε'') part of the dielectric permittivity of $Ho_2Ti_2O_7$ (a, b) and $Dy_2Ti_2O_7$ (c, d) measured at different frequencies.

To describe the nature of relaxation in HTO as well as in DTO, we determined the critical exponent γ using the above equation 3.1. Figure 3.3 (a) and (b) shows the plots of ln $(\frac{1}{\varepsilon'} - \frac{1}{\varepsilon'_m})$ as a function of ln $(T-T_{m'})$ for 90 K and 36 K relaxation at 1 kHz frequency (with the calculated values of diffusivity constant γ) for both HTO and DTO.

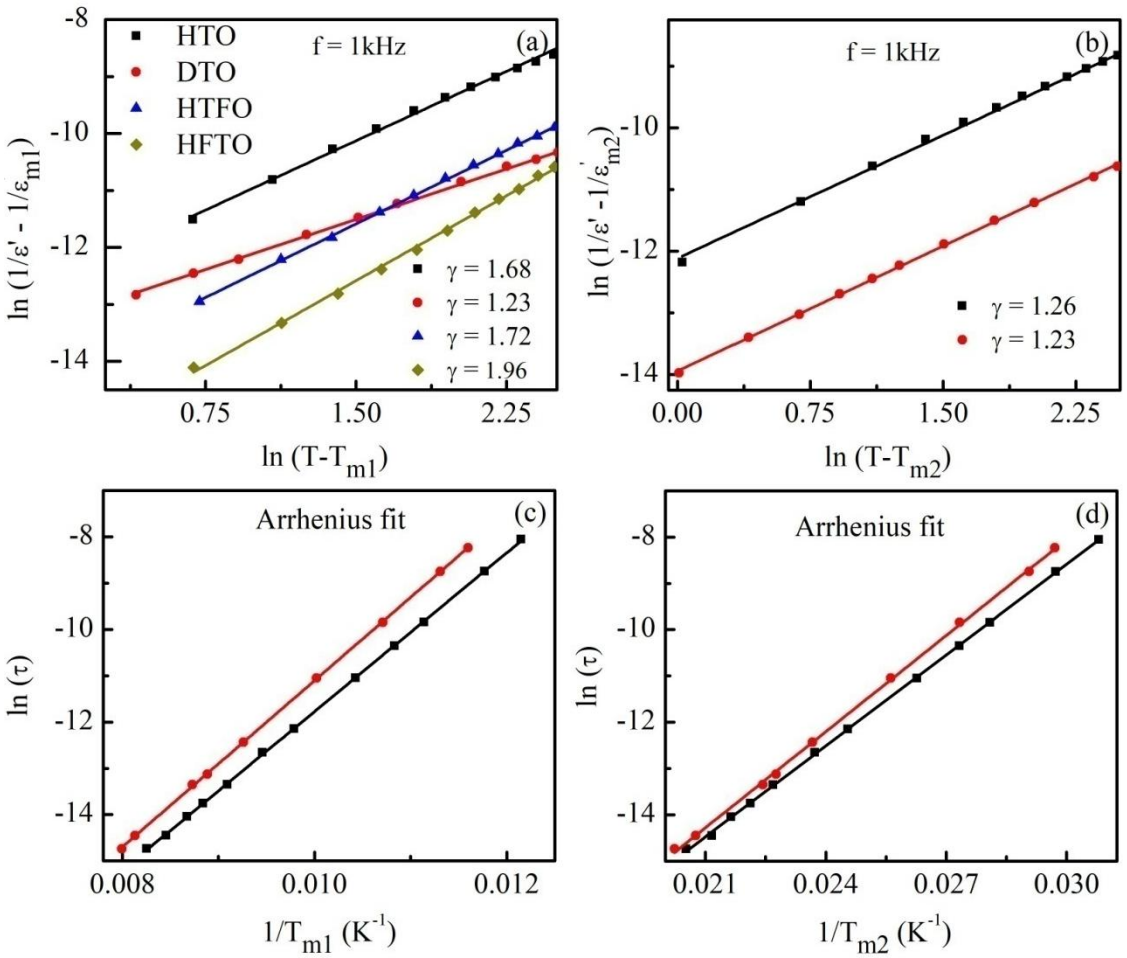

Figure 3.3: Plot of ln $(1/\varepsilon' - 1/\varepsilon_{m'})$ as a function of ln $(T-T_{m'})$ at 1 kHz for 90 K relaxations for $Ho_2Ti_2O_7$, $Dy_2Ti_2O_7$, $Ho_2Ti_{1.85}Fe_{0.15}O_7$ & $Ho_{1.8}Fe_{0.2}Ti_2O_7$ (a) and 36 K relaxations for $Ho_2Ti_2O_7$ & $Dy_2Ti_2O_7$ (b). ln (τ) vs. $1/T_{m''}$ plot with Arrhenius fit for 90 K (c) and 36 K relaxation observed in $Ho_2Ti_2O_7$ and $Dy_2Ti_2O_7$.

As mentioned earlier, there are two dielectric relaxations for both HTO and DTO. For HTO, the deduced value of γ is 1.68 and 1.26 for the dielectric relaxation occurring at 90 K and 36 K respectively. For DTO, the value of γ turns out to be 1.23 for both relaxations, occurring at 92.5 K and 37 K. The so obtained values of γ confirm that both observed dielectric relaxations are diffusive in nature for both the compounds. Diffusive nature of relaxation is generally associated from the subtle change or rearrangement of the bonds of the particular sites of the crystal structure without breaking lattice periodicity. Since, unlike the other diffuse or relaxor compounds, HTO and DTO do not contain any chemical disorder. This suggests that both observed diffuse relaxations are inherently generated by the lattice.

In order to investigate the nature of frequency dispersion behavior of both relaxations, ln (τ) vs. $1/T_{m''}$ plot has been fitted using the Arrhenius equation, $\tau = \boldsymbol{\tau_0} \exp\left(\frac{Ea}{KT}\right)$. Where τ is the measuring relaxation time in sec, $\boldsymbol{\tau_0}$ is the characteristic relaxation time, and E_a is activation energy given in unit of meV. Plot of ln (τ) vs. $1/T_{m''}$ with linear fit for both 90 K and 36 K relaxation of HTO and DTO has been shown in Figure 3.3 (c) & (d). The obtained values of E_a and $\boldsymbol{\tau_0}$ for HTO and DTO are summarized in table 3.2.

Table 3.2: Value of activation energy E_a (meV) and characteristic relaxation time $\boldsymbol{\tau_0}$ (sec) for 90 K and 36 K relaxations deduced from- peak position $T_{m''}$ of temperature dependent ε'' and Lacroix-Béné function fitted obtained parameters τ_0 (in the bracket.).

Compound	T_{m1}		T_{m2}	
	E_a (meV)	$\boldsymbol{\tau_0}$ (sec)	E_a (meV)	$\boldsymbol{\tau_0}$ (sec)
HTO	147.2±0.2 (139.8±3)	2.9×10^{-13} (7.0×10^{-13})	56.5±0.2 (50.0±2)	5.5×10^{-13} (3.8×10^{-12})
DTO	155.8±0.2 (138.2±3)	2.1×10^{-13} (1.7×10^{-12})	60.1±0.2 (52.4±1.2)	2.7×10^{-13} (2.4×10^{-12})

Furthermore, nature of both relaxations of both of HTO and DTO has been investigated in terms of frequency-dependent variation of the dielectric permittivity at fixed temperature. To illustrate the frequency dependence of the dielectric permittivity at fixed temperature we have replotted the figure 3.2. Figure 3.4 shows the frequency dependence of the real and imaginary part of the dielectric permittivity at different temperature for both HTO and DTO. It has been found that on increasing temperature, both relaxation peak observed in ε'' shifted towards the higher frequency side in both compounds. This temperature-dependent variation of the relaxation peak suggests the thermally activated relaxation mechanism.

To investigate the nature of relaxation, we fit the ε' vs. f data by using Lacroix- *Béné*-type distribution function of relaxation time, $\tau = 1/2\pi f$ given by [112]

$$G(\ln \tau) = \frac{\sin(\pi\beta)}{\pi} \left(\frac{\tau_0}{\tau - \tau_0}\right)^{\beta} \qquad \text{for } \tau > \tau_0$$

And (3.2)

$$G(\ln \tau) = 0 \qquad \text{for } \tau < \tau_0$$

The values of τ_0 and β determines the fastest relaxation time and polydispersivity of the system. For monodispersitive system one obtained $\beta = 1$. In terms of τ_0 and β, the complex dielectric permittivity of polydispersive system becomes

$$\tilde{\varepsilon}(\omega) = \varepsilon_s - (\varepsilon_s - \varepsilon_\infty)\left(1 + \frac{1}{i\omega\tau_0}\right)^{-\beta} \qquad (3.3)$$

Where, $\omega = 2\pi f$ and ε_s, ε_∞ are the static and high limit-f of ε', respectively.

In terms of ε' and ε'' the expression becomes

$$\varepsilon' = \varepsilon_s - (\varepsilon_s - \varepsilon_\infty)(\cos\lambda)^\beta \cos\lambda\beta \qquad 3.4\ (a)$$

$$\varepsilon'' = (\varepsilon_s - \varepsilon_\infty)(\cos\lambda)^\beta \sin\lambda\beta \qquad 3.4\ (b)$$

Where, $\lambda = \text{arccot}(\omega\tau_0)$

Figure 3.5 shows the best fit of ε' vs. f plot of both compounds using equation 3.4 (a) whereas the parameters- ε_s, ε_∞, β and τ_0 obtained from fitting are listed in table 3.4. The observed values of β for both relaxations lies between 0.85-0.95 ranges (close to 1), suggesting the monodispersive Debye-like nature of relaxations. With the help of obtained values of τ_0, we plot the ln (τ) vs. 1/T to reconfirm the Arrhenius nature and activation energy of both relaxations observed in HTO and DTO. Inset of figure 3.5 shows the plot of ln (τ) vs. 1/T with linear fit whereas the obtained values of characteristic relaxation time ($\boldsymbol{\tau_0}$) and activation energy (E_a) are listed in table 3.3 (in the bracket).

Table 3.3: Obtained values of fitting parameters ε_s, ε_∞, β, and τ_0 referring to the dispersion data ε' of figure 6 for $Ho_2Ti_2O_7$ and $Dy_2Ti_2O_7$.

$Ho_2Ti_2O_7$					$Dy_2Ti_2O_7$				
T (K)	ε_s	ε_∞	β	τ_0 (s)	T (K)	ε_s	ε_∞	β	τ_0 (s)
33	50.59(1)	50.28(1)	0.90(1)	1.68×10^{-4}	34	82.34(2)	82.30(2)	0.93(1)	1.48×10^{-4}
35	50.63(1)	50.22(1)	0.88(1)	6.12×10^{-5}	36	82.33(1)	82.27(1)	0.92(4)	5.87×10^{-5}
37	50.60(1)	50.16(0)	0.86(3)	2.46×10^{-5}	38	82.30(1)	82.25(1)	0.92(2)	2.18×10^{-5}
39	50.55(1)	50.12(0)	0.85(1)	1.12×10^{-5}	40	82.28(2)	82.22(1)	0.92(1)	1.03×10^{-6}
85	50.19(3)	48.70(1)	0.95(1)	1.06×10^{-4}	85	81.58(1)	81.43(1)	0.94(1)	2.46×10^{-4}
88	50.10(2)	48.56(2)	0.94(1)	5.66×10^{-5}	88	81.56(1)	81.36(1)	0.93(5)	1.44×10^{-4}
91	50.08(2)	48.41(2)	0.92(1)	3.28×10^{-5}	91	81.51(2)	81.30(3)	0.93(2)	7.94×10^{-5}
94	49.88(2)	48.23(2)	0.89(4)	1.89×10^{-5}	94	81.45(3)	81.24(1)	0.92(4)	4.51×10^{-5}
97	49.73(1)	48.06(2)	0.85(3)	1.07×10^{-5}	97	81.39(1)	81.17(1)	0.92(2)	2.52×10^{-5}
					100	81.33(4)	81.11(1)	0.92(2)	1.49×10^{-5}

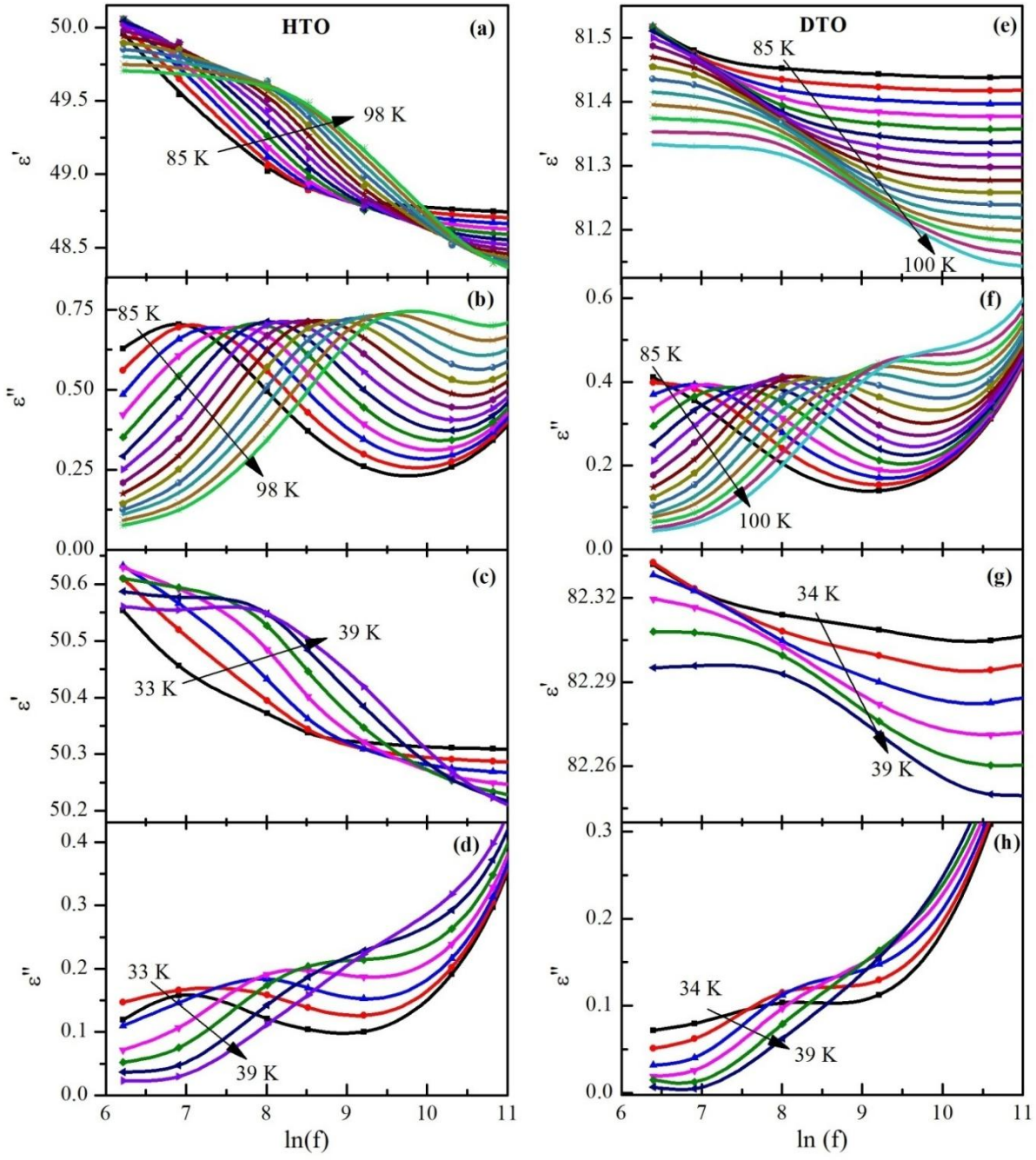

Figure 3.4: Frequency dependence of the real (ε') and imaginary (ε'') part of the dielectric permittivity of $Ho_2Ti_2O_7$ (a, b, c and d) and $Dy_2Ti_2O_7$ (e, f, g and h) at different temperatures.

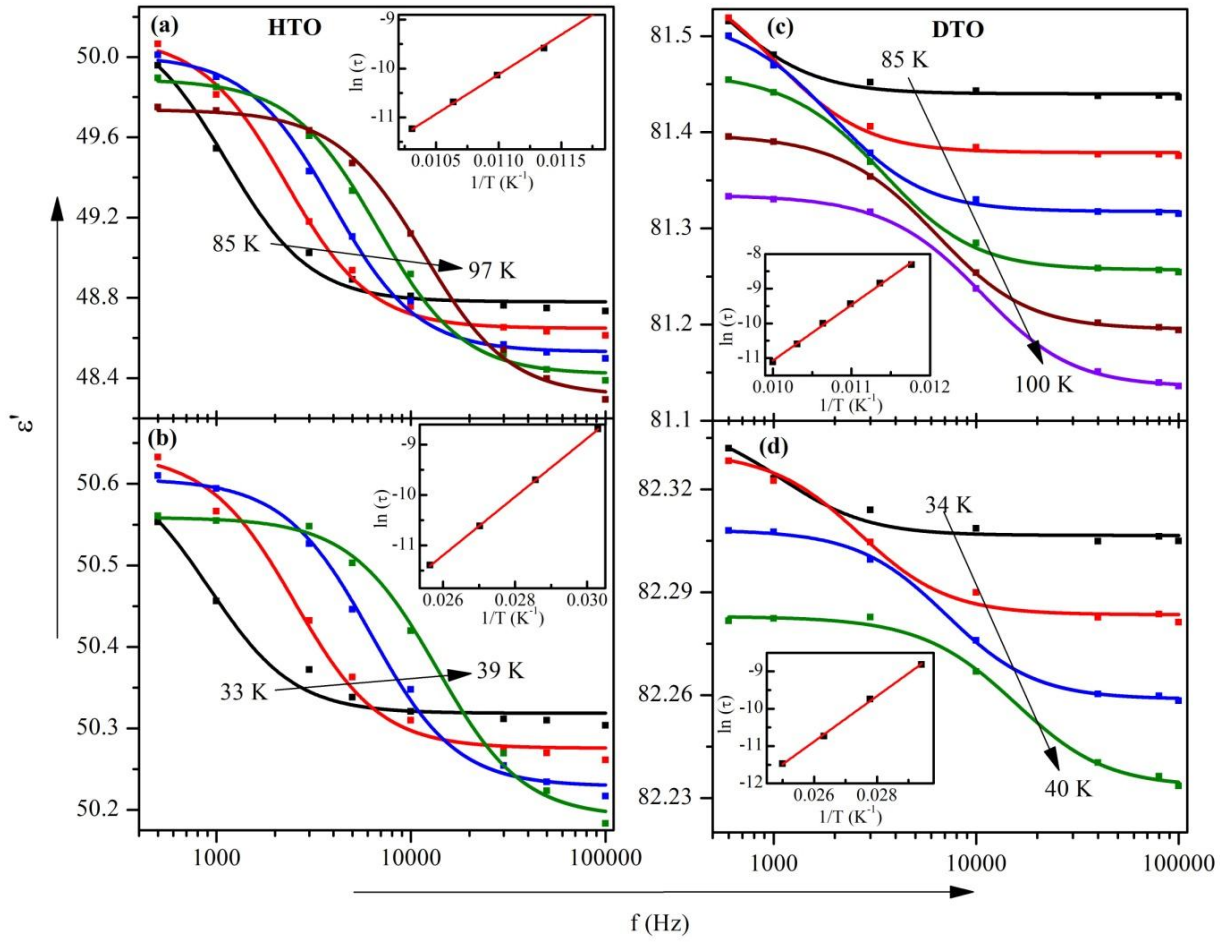

Figure 3.5: Lacroix-Béné function fit of ε' vs. f plot at different temperatures of $Ho_2Ti_2O_7$ (a, b) and $Dy_2Ti_2O_7$ (c, d). Inset shows the Arrhenius fitted ln (τ_0) vs. 1/T plot.

The analysis of frequency-dependent dielectric permittivity reconfirms that both 90 K and 36 K relaxation observed in both HTO and DTO are thermally activated, having similar order of characteristic relaxation time and activation energy as obtained from temperature dependent dielectric permittivity studies. It has been found that the observed value of characteristic relaxation time for both relaxations have the same order but having different value of activation energies. Relaxation time originating from polar lattice vibrational effects lies in the range of 10^{-9}-10^{-14} sec. In case of HTO and DTO, deduced value of τ_0 is found in the

range of 10^{-12}-10^{-13} sec. This suggests that observed relaxations in HTO and DTO are related to polar lattice vibrational effects originating from the local distortions. The order of characteristic relaxation time and activation energy as obtained by Arrhenius fit are well correlated with other relaxor phase transition e.g. $Bi_{1.5}Zn_{1.0}Nb_{1.5}O_7$ and Bi_2O_3–ZnO–Nb_2O_5 cubic pyrochlores [113], [114]. In these studies; it has been concluded that dielectric relaxation is originated by local distortions in oxygen positions and influenced by phonon branches associated with O1-A-O1 and O2-A-O2 bending modes. In the present study of HTO and DTO, the order of activation energy is ~150 meV and ~50 meV for 90 K and 36 K relaxations, respectively. In congruence with the activation energy and assigned phonon modes in ref. [113], [114], it may be concluded that 90 K diffused phase relaxation is originated by local structural distortion in O1 site oxygen position and must be influenced by phonon branches associated with O1-A-O1 bending modes and 36 K relaxation is originated by local structural distortion in O2 site oxygen position and influenced by the phonon branches associated with O2-A-O2 bending modes. Moreover, if both relaxations is distinctly related to O1 and O2 crystallographic site of the oxygen position then as structure suggests (figure 1.8), distortion at B-site only affect 90 K relaxation whereas A-site distortion affects both relaxations. In order to confirm the origin of each relaxation, chemical inhomogeneity at B-site (Ti-site) and A-site (Ho-site) through Fe-substitution has been created and their effects are studied in detail.

3.2.2.1 B-site doped $Ho_2Ti_{1.85}Fe_{0.15}O_7$

Temperature dependence of dielectric permittivity of B-site doped HTFO sample is shown in figure 3.6 (a) & (b). For 10 KHz frequency the y-scale values of ε" lies the range of 0.07-0.25. The offset value for 10 kHz and 300 kHz varied from 0.01 to 2.0. Out of the two

relaxations of HTO, only 90 K relaxation is getting affected by this partial substitution. The nature of relaxation has also changed quite significantly. The narrower relaxation present in case of HTO has broadened as well as frequency dispersion smeared out over a wide temperature range. The measured value of γ (at 1 kHz) for HTFO has changed to 1.72 from 1.67 for HTO as shown in figure 3.3(a). The higher value of γ shows that the observed phase relaxation is shifting towards a relaxor type but still can be categorized as diffusive in nature.

3.2.2.2 A-site doped $Ho_{1.8}Fe_{0.2}Ti_2O_7$

The temperature dependent dielectric permittivity of A-site doped HFTO samples is shown in figure 3.6 (c) & (d). For 10 KHz frequency the y-scale values of ε" lies the range of 0.01-1.5. The offset value for 10 kHz and 300 kHz varied from 0.01 to 0.2. It is found that A-site Fe doping affects both relaxation temperatures and almost a single relaxation is observed in place of two relaxations in ε' and ε". The measured value of γ (at 1 kHz) for HFTO turns out to be 1.96 as indicated in figure 3.3 (a). This shows that this relaxation becomes almost relaxor-like [111], [115].

Table 3.4: Observed values of bond length and bond angle of $Ho_2Ti_2O_7$, $Dy_2Ti_2O_7$, $Ho_2Ti_{1.85}Fe_{0.15}O_7$ and $Ho_{1.8}Fe_{0.2}Ti_2O_7$ obtained from Rietveld refinement.

Compound	Bond length (Å)			Bond angle (^{0})		
	A-O2	A-O1	B-O1	O2-A-O2	O1-A-O1	O1-B-O1
HTO	2.1868(4)	2.519(3)	1.9361(12)	180(0)	62.88(3)	85.47(12)
DTO	2.1925(5)	2.553(3)	1.9262(15)	180(0)	62.53(4)	86.95(16)
HTFO	2.1870(0)	2.5127(15)	1.9397(8)	180(0)	62.964(19)	85.14(8)
HFTO	2.1824(6)	2.496(3)	1.9421(17)	180(0)	63.12(4)	84.55(15)

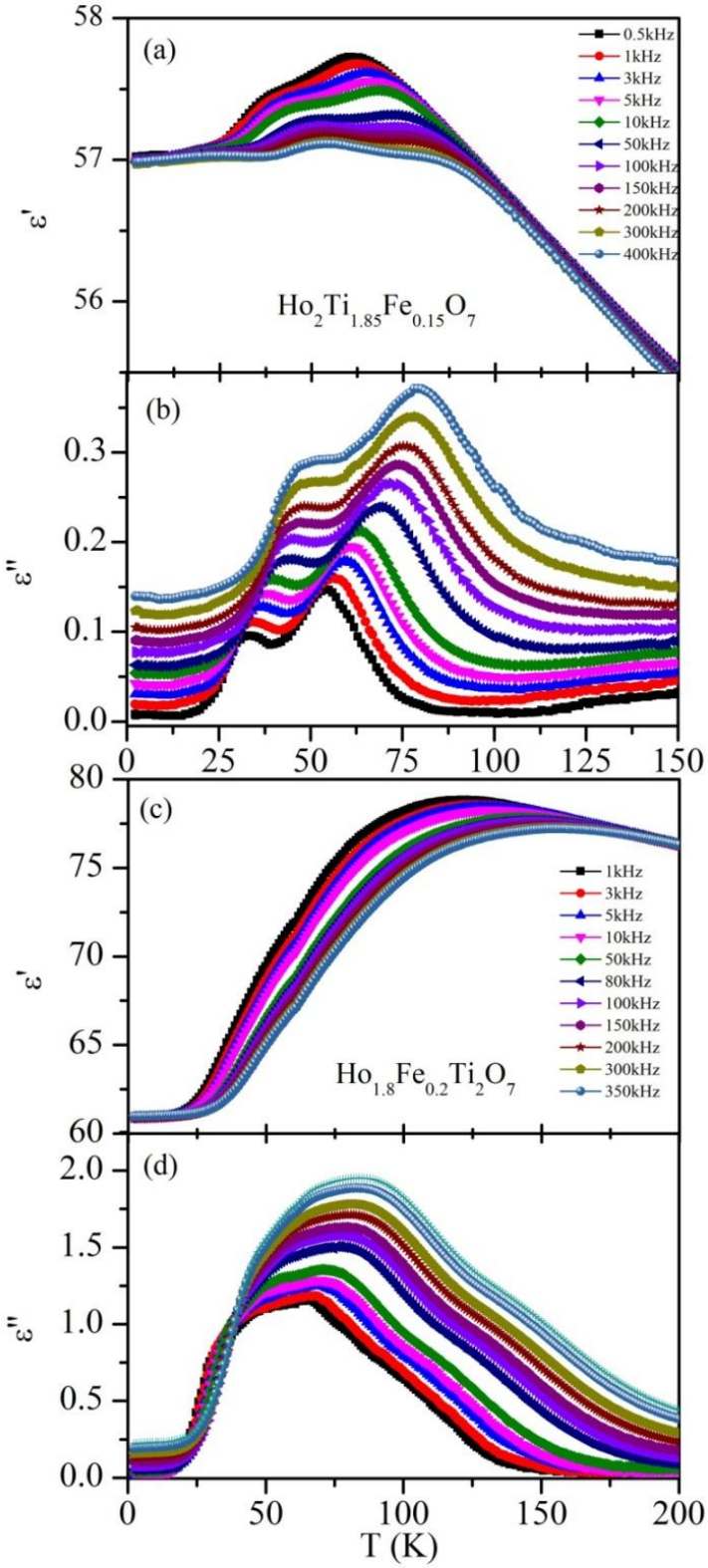

Figure 3.6: Temperature dependence of the real (ε') and imaginary (ε'') part of the dielectric permittivity of $Ho_2Ti_{1.85}Fe_{0.15}O_7$ (a, b) and $Ho_{1.8}Fe_{0.2}Ti_2O_7$ (c, d) measured at different frequencies.

The structural data obtained from the Rietveld refinement has been used for calculation of bond length and bond angle between the A/B sites with associated oxygen as shown in figure 1.8. Table 3.4 lists the details of these bond length and bond angles. It has been found that for B-site substituted $Ho_2Ti_{1.85}Fe_{0.15}O_7$ (HTFO) sample, only A/B-O1 bond lengths, and O1-A/B-O1 bond angles are getting affected whereas A-O2 bond length and O2-A-O2 bond angle are nearly unaffected (table 3.4). Contrary to that, for A-site Fe substituted $Ho_{1.8}Fe_{0.2}Ti_2O_7$ (HFTO) sample A/B-O1, as well as A-O2 bond lengths, are affected with a change in O1-A/B-O1 bond angle as well. These results suggests, in HTO and DTO, diffused dielectric relaxations prevailing at 90 K and 36 K originates from the distortion in the O1 and O2 oxygen site, respectively. A similar kind of finding has been confirmed by temperature dependent Raman, crystal field excitation and principle elastic constant studies by Mączka et al. [96], Lummen et al. [116] and Nakanishi et al. [117]. It has been shown that at low temperature (<120 K), a structural distortion in both oxygen position takes place via softening in F_{2g} phonon mode related to O1 and O2 site of oxygen position.

In $Fd\bar{3}m$ space group, a gyrotropic order which belongs to A_{1u} irreducible representation of O_h point group is not compatible with any phonon mode related to the structural order parameters. This clearly indicates that observed transitions can have only an electronic origin [97]. In these RE compounds, crystal field anisotropy splits the five component multipolar order parameter Q_{ij}, into two-dimensional E_u representation ($Q_{xx} - Q_{yy}$, $2Q_{zz} - Q_{xx} - Q_{yy}$) and a three-dimensional T_{2u} representation (Q_{xy}, Q_{yz}, Q_{zx}) [118], [119]. The splitting of electronic order parameters, which is also responsible for the Ising nature of Ho/Dy spin, are more prominent below 120 K [120]. In neutron scattering and nuclear quadrupole resonance (^{47}Ti-NQR) experiments, a nonmonotonic increment in the spin relaxation time has been observed

below 120 K by Clancy et al. [71], Kitagawa et al. [121] and Almog et al. [120] as well. Whereas, in temperature-dependent crystal field excitations studies, it has been observed that below 130 K, various crystal field excitations emerges which get coupled with the phononic excitations [52], [94], [116], [122]. These observations indicate the interconnection between the splitting of multipolar order parameters and structural distortion at the oxygen position. It can be suggested that E_u and T_{2u} electronic order parameter are coupled with the F_{2g} structural order parameters [123]. Furthermore, the splitting of multipolar order parameters and its associated structural distortions are observed below 130 K. This suggests that acting crystal field becomes more pronounced below 130 K and due to the coupling of structural order parameters with electronic order parameters, a change in the lattice volume should be occur at low temperature in these compounds.

3.2.3 Low temperature structural analysis

To confirm this change in the lattice volume, the low-temperature synchrotron x-ray diffraction (SRXRD) measurement of HTO and DTO is presented here. Figure 3.7 shows the SRXRD pattern of HTO and DTO measured at different temperature. In the measured temperature range; it has been found that SRXRD patterns do not show any structural transition which confirms that similar to high temperature these compounds pertain its $Fd\bar{3}m$ space group at low temperatures as well. Figure 3.8 shows the selected Rietveld refinement profile of SRXRD data of HTO and DTO measured at 150 K, 70 K, 30 K and 15 K. The details of the structural and fitting parameters of the Rietveld refinement of HTO and DTO are listed in table 3.5 and 3.6, respectively. Figure 3.9 shows the temperature-dependent variation of lattice volume of HTO and DTO. It has been found that on decreasing

temperature lattice volume decreases up to 30 K, whereas below this temperature an anomalous increment in the lattice volume takes place in both the compounds.

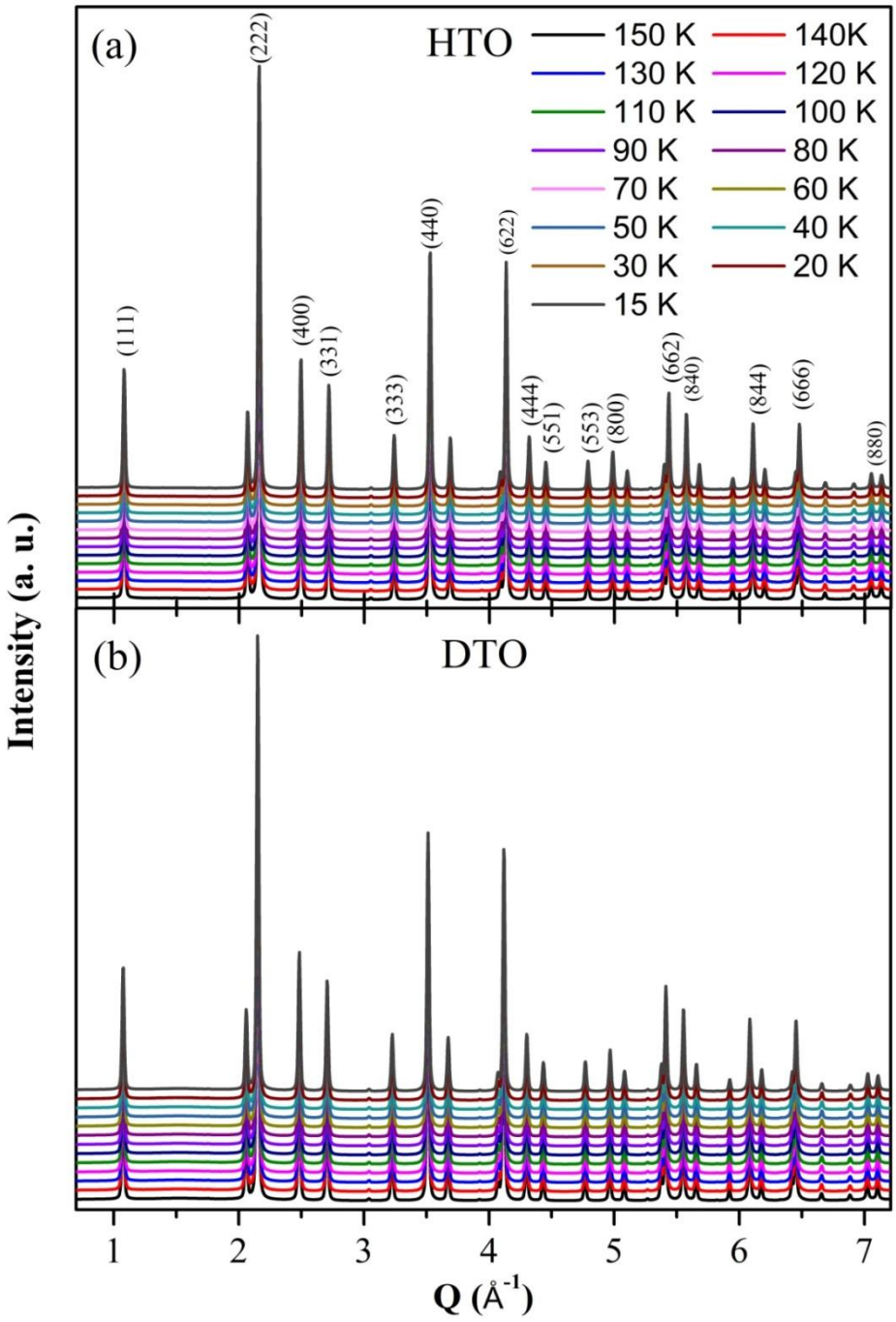

Figure 3.7: Synchrotron x-ray diffraction (SRXRD) pattern of polycrystalline (a) $Ho_2Ti_2O_7$ and (b) $Dy_2Ti_2O_7$ measured at different temperatures.

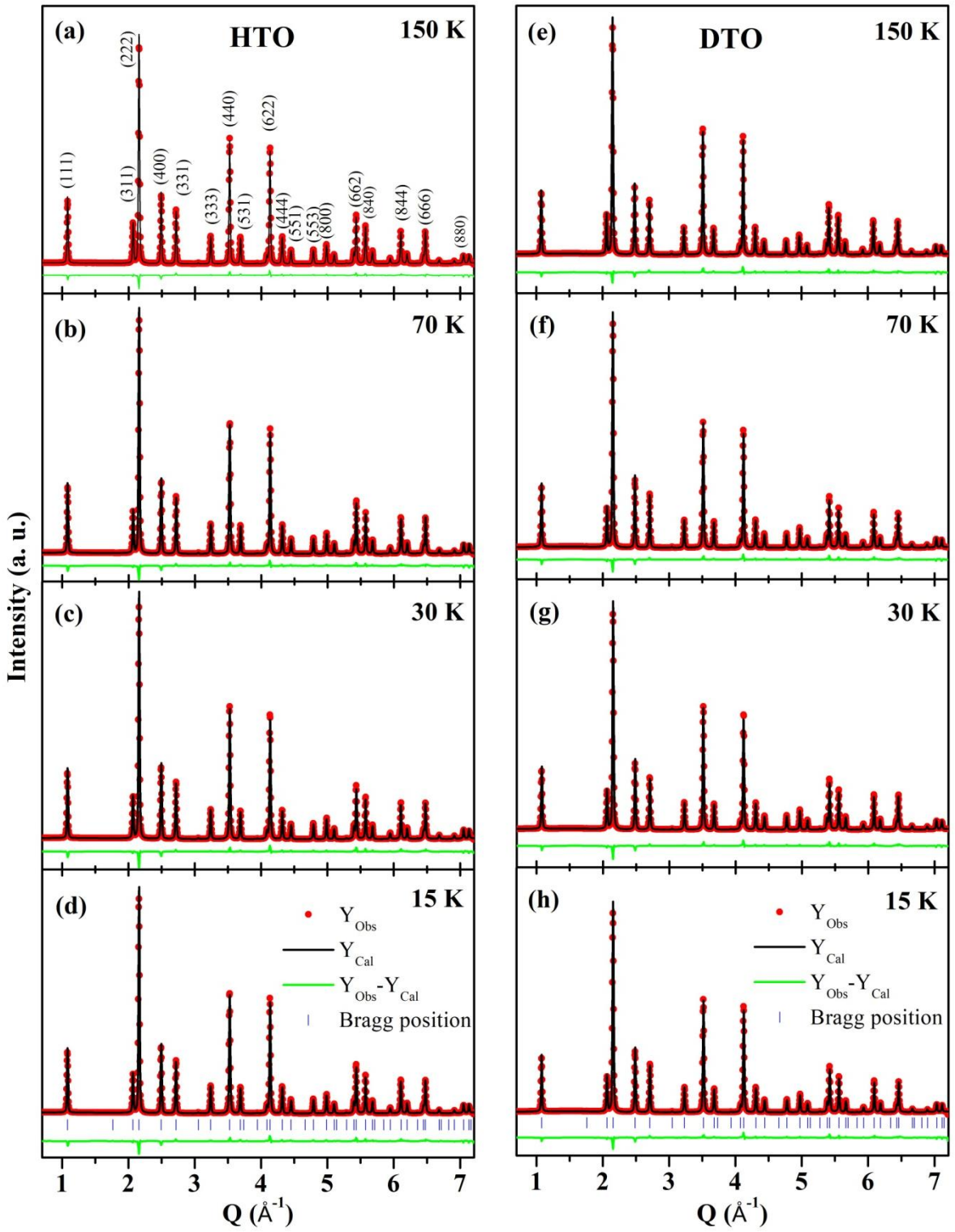

Figure 3.8: Rietveld refinement of Synchrotron x-ray diffraction pattern of polycrystalline $Ho_2Ti_2O_7$ (a, b c, and d) and $Dy_2Ti_2O_7$ (e, f, g, and h) measured at 150K, 110 K, 70 K and 30 K.

Table 3.5: Details of crystallographic parameters and goodness of fit as obtained from Rietveld refinement of low temperature synchrotron x-ray diffraction $Ho_2Ti_2O_7$.

T (K)	a (Å)	*x (48 f)*	R_p	R_{wp}	R_{exp}	χ^2
150	10.0847(1)	0.3283(3)	4.56	5.65	5.16	1.19
140	10.0839(1)	0.3283(3)	4.66	5.74	5.12	1.25
130	10.0832(1)	0.3283(3)	4.71	5.80	5.06	1.31
120	10.0826(1)	0.3283(3)	4.76	5.84	4.96	1.38
110	10.0819(1)	0.3283(3)	4.78	5.84	4.84	1.45
100	10.0813(1)	0.3283(3)	4.91	6.01	4.87	1.52
90	10.0808(1)	0.3282(3)	4.80	5.91	4.67	1.60
80	10.0804(1)	0.3282(3)	4.88	5.99	4.66	1.65
70	10.0800(1)	0.3282(3)	4.93	6.07	4.66	1.69
60	10.0795(1)	0.3282(3)	5.00	6.16	4.64	1.76
50	10.0792(1)	0.3283(3)	5.13	6.25	4.65	1.81
40	10.0789(1)	0.3283(3)	5.37	6.44	4.82	1.78
30	10.0788(1)	0.3283(3)	5.56	6.53	4.99	1.71
20	10.0798(1)	0.3282(3)	5.18	6.20	4.73	1.71
15	10.0802(1)	0.3281(3)	5.04	6.04	4.69	1.66

Table 3.6: Details of crystallographic parameters and goodness of fit as obtained from Rietveld refinement of low temperature synchrotron x-ray diffraction $Dy_2Ti_2O_7$.

T (K)	A (Å)	*x (48 f)*	R_p	R_{wp}	R_e	χ^2
150	10.1109(1)	0.3276(1)	4.91	5.24	4.90	1.14
140	10.1101(1)	0.3276(1)	5.07	5.41	4.93	1.20
130	10.1094(1)	0.3276(1)	5.10	5.44	4.94	1.21
120	10.1087(1)	0.3277(0)	5.13	5.46	4.96	1.21
110	10.1081(1)	0.3278(1)	5.19	5.52	4.98	1.23
100	10.1076(1)	0.3278(3)	5.32	5.65	4.99	1.28
90	10.1071(1)	0.3279(1)	5.45	5.76	5.07	1.29
80	10.1066(1)	0.3277(2)	5.46	5.80	4.86	1.42
70	10.1062(1)	0.3276(1)	5.48	5.85	4.71	1.54
60	10.1058(1)	0.3277(3)	5.65	6.04	4.90	1.52
50	10.1054(1)	0.3278(1)	5.77	6.14	4.88	1.58
40	10.1049(1)	0.3279(1)	5.77	6.19	5.00	1.53
30	10.1045(1)	0.3278(1)	5.90	6.30	4.89	1.66
20	10.1056(1)	0.3278(3)	5.77	6.06	4.97	1.45
15	10.1061(1)	0.3278(1)	5.49	5.80	4.95	1.37

To extract the crystal field induced change in the lattice volume, the data was fitted using Debye-Grüneisen equation, accounting the anharmonic parts of lattice vibration due to thermal expansion [124], [125].

$$V \cong V\,(T=0) + \int_0^T \frac{\gamma' C_v}{B}\,dT \cong V\,(T=0) + \frac{9\gamma' N k_B}{B} T \left(\frac{T}{\Theta_D}\right)^3 \int_0^{\Theta_D/T} \frac{x^3}{e^x - 1}\,dx \qquad (3.5)$$

Where, V (T=0), Θ_D, γ' and B represents the volume at 0 K, Debye temperature, the Grüneisen parameters and bulk modulus respectively. V (T=0), Θ_D and $\frac{9\gamma' N k_B}{B}$ are the fitting parameters which have been determined by fitting the data in 150 to 70 K temperature range. The obtained values of V (T=0), Θ_D and $\frac{9\gamma' N k_B}{B}$ are 1023.99± 0.01 $Å^3$, 378.1± 12.8 K and 0.093± 0.003 for HTO whereas 1031.92± 0.03 $Å^3$, 337.8± 19.0 K and 0.085± 0.004, for DTO, respectively. The obtained fitting has been extrapolated for low temperatures and represented as a solid line in figure 3.9. It has been found that the obtained value of Debye temperature for DTO is similar as obtained by Hiroi et al. from specific heat measurement, which confirms the correctness of the Debye fit [126]. The fitted temperature-dependent lattice volume of HTO and DTO shows a clear deviation below ~70 K from Debye behavior. This observation is further confirming the prominence of crystal field at low temperature induces structural distortion in these compounds.

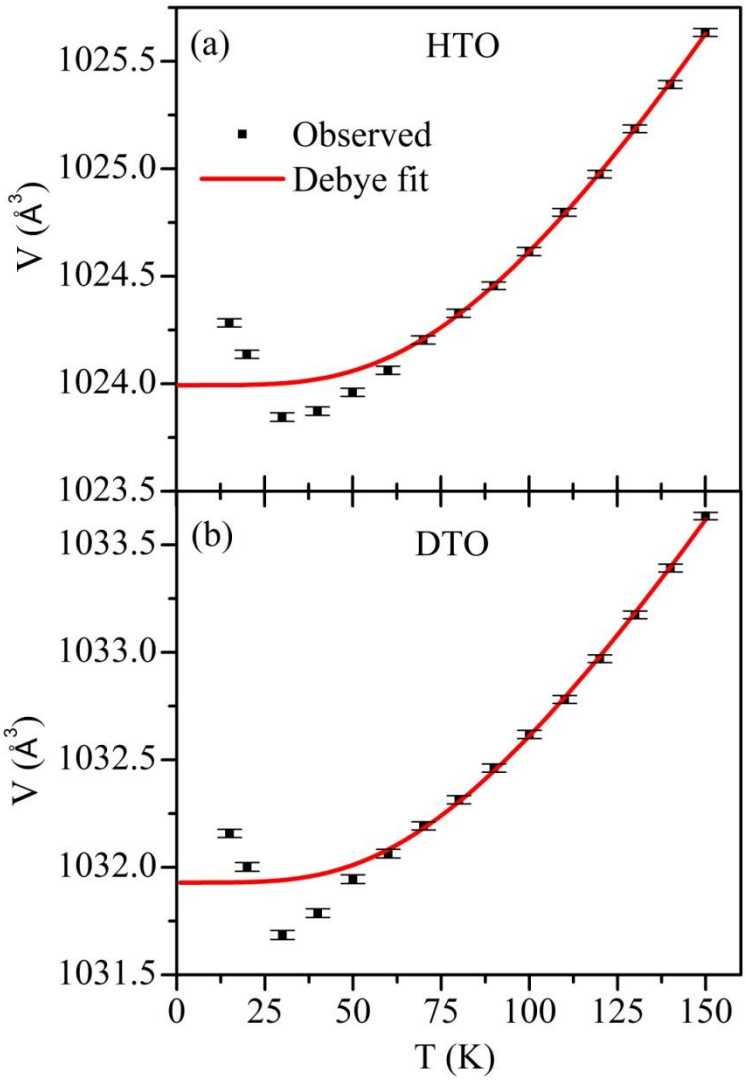

Figure 3.9: Temperature dependent variation of the lattice volume (dot) and modeled Debye – grüneisen fit (solid red line) for (a) $Ho_2Ti_2O_7$ and (b) $Dy_2Ti_2O_7$.

3.3 Conclusion

Temperature-dependent dielectric measurement shows two distinct relaxations around 90K and 36K in both $Ho_2Ti_2O_7$ and $Dy_2Ti_2O_7$ spin ice compound. Obtained value of critical exponent in Curie-Weiss and Lacroix- *Béné* fitting of relative dielectric permittivity indicates that both relaxations are diffusive and Debye-like in nature. The value of activation energy

(E_a), dielectric response and structural analysis of A & B-site doped $Ho_2Ti_2O_7$ shows that both relaxations at 90K and 36K are inherently related to the lattice distortions at O1 (48f) and O2 (8b) sites of structure. The low temperature synchrotron x-ray diffraction studies show deviation in the lattice volume from Debye – grüneisen behaviour at low temperature without any structural phase transition. This confirms the absence of ferroelectric phase transitions. In these spin ices; crystal field anisotropy splits the multipolar order parameter, which is coupled with the structural order parameters. It has been suggested that at low temperature, crystal field becomes pronounced as observed in previously crystal field excitations, Raman, neutron and nuclear quadrupole resonance (^{47}Ti-NQR) studies. Due to coupling between the multipolar and structural order parameters, this pronounced change in crystal electric field induces structural distortion at O1 and O2 sites of the oxygen position without breaking the crystal symmetries, reflected in the form of dielectric relaxation in these compounds. These results determine the nature and possible cause of the dielectric relaxations prevailing in these spin ice compounds.